

# Temporal correlations of superconductivity above the transition temperature in $\text{La}_{2-x}\text{Sr}_x\text{CuO}_4$ probed by terahertz spectroscopy

L. S. Bilbro<sup>1</sup>, R. Valdés Aguilar<sup>1</sup>, G. Logvenov<sup>2</sup>, O. Pelleg<sup>2</sup>, I. Božović<sup>2</sup> and N. P. Armitage<sup>1\*</sup>

**The nature of the underdoped pseudogap regime of the high-temperature copper oxide superconductors has been a matter of long-term debate<sup>1–3</sup>. On quite general grounds, we expect that, owing to their low superfluid densities and short correlation lengths, superconducting fluctuations will be significant for transport and thermodynamic properties in this part of the phase diagram<sup>4,5</sup>. Although there is ample experimental evidence for such correlations, there has been disagreement about how high in temperature they may persist, their role in the phenomenology of the pseudogap and their significance for understanding high-temperature superconductivity<sup>6–10</sup>. Here we use THz time-domain spectroscopy to probe the temporal fluctuations of superconductivity above the critical temperature ( $T_c$ ) in  $\text{La}_{2-x}\text{Sr}_x\text{CuO}_4$  (LSCO) thin films over a doping range that spans almost the entire superconducting dome ( $x = 0.09–0.25$ ). Signatures of the fluctuations persist in the conductivity in a comparatively narrow temperature range, at most 16 K above  $T_c$ . Our measurements show that superconducting correlations do not make an appreciable contribution to the charge-transport anomalies of the pseudogap in LSCO at temperatures well above  $T_c$ .**

In general, continuous phase transitions are typified by fluctuations with correlation length and timescales that diverge near  $T_c$ . Dynamical measurements such as THz time-domain spectroscopy are sensitive probes of the onset of superconductivity<sup>11</sup> and measure its temporal correlations on the timescales of interest. In the presence of superconducting vortices such high-frequency measurements are not affected by effects such as vortex pinning, creep and edge barriers, which often complicate interpretation of low-frequency and d.c. results. In this study, we investigate the fluctuation superconductivity in thin films of LSCO grown by molecular beam epitaxy. This synthesis technique provides exquisite control of the thickness and chemical composition of the films; the intrinsic chemical tunability of LSCO enables us to investigate essentially the entire phase diagram. For details on the films, see Supplementary Information.

In Fig. 1a and b, we show the real ( $\sigma_1$ ) and imaginary ( $\sigma_2$ ) parts of the THz conductivity measured at a number of different temperatures for optimally doped LSCO ( $x = 0.16$ ) with  $T_c = 41$  K. We obtain similar data at other doping levels. The spectra are easily understood in the limiting cases of high and low temperatures. Well above the onset of superconductivity, the real part of the conductivity is almost frequency independent and the imaginary part is small, consistent with the expected behaviour of a metal at frequencies well below the normal-state scattering rate. At

the lowest temperature the conductivity is consistent with that expected for a long-range ordered superconductor;  $\sigma_1$  is small as most of the low-frequency spectral weight has condensed into the  $\omega = 0$  delta function, and the frequency dependence of  $\sigma_2$  is very close to  $1/\omega$ . Our principal interest, however, is in the interesting transition region around  $T_c$ , where fluctuations of superconductivity are apparent. Here, both components of the conductivity are enhanced, with  $\sigma_1$  first rising and then falling as spectral weight moves to frequencies below the measurement range in the superconducting state.

The fluctuation regime is perhaps most evident in Fig. 1c,d, where we plot the complex conductivity of the same sample as a function of temperature. Above the transition, the real conductivity shows a slow decrease as the temperature is raised, consistent with the increasing normal-state d.c. resistivity. Near  $T_c$  a ‘loss peak’ occurs owing to the onset of strong superconducting fluctuations; it is exhibited at progressively lower temperatures as the probing frequency is decreased (inset to Fig. 1c). As discussed below, this is a direct consequence of the slowing down of superconducting fluctuations as  $T$  is lowered. About 10 K above  $T_c$ , the imaginary conductivity shows a sharp upturn at low frequency (inset to Fig. 1d), indicating the onset of strong superconducting correlations<sup>11,12</sup>. Whether such correlations persist well above the 10–15 K range above  $T_c$  is a more subtle issue, which we discuss below. For all dopings, the region of obvious enhancement is far below the temperature of the diamagnetism and Nernst onset measured in LSCO crystals<sup>7,10,13</sup>, but is consistent with the onset found in other a.c. conductivity studies<sup>11,14–17</sup>.

An important quantity for understanding superconducting fluctuations is the phase stiffness, which is the energy scale for introducing twists in the phase  $\phi$  of the complex superconducting order parameter  $\Delta e^{i\phi(r)}$ . As in any continuous elastic medium we can write the energy of a phase deformation in the form of  $E = (\mathcal{T}_\phi (\nabla\phi)^2)/2$  where  $\mathcal{T}_\phi$  is a stiffness constant. As a phase gradient is associated with a superfluid velocity, this ‘elastic’ energy is equivalent to the centre-of-mass kinetic energy. For  $N$  particles of mass  $m$ , the stiffness is  $\mathcal{T}_\phi = (N\hbar^2)/m$ . We can measure this quantity directly through the imaginary part of the fluctuation conductivity  $\sigma_{2f}$ , as  $k_B T_\phi = (\hbar\omega\sigma_{2f}t)/G_Q$ . Here  $T_\phi$  is the two-dimensional stiffness of a single  $\text{CuO}_2$  plane given in units of degrees Kelvin,  $G_Q = e^2/\hbar$  is the quantum of conductance and  $t$  is the inter- $\text{CuO}_2$  plane spacing. The phase stiffness is usually regarded as an equilibrium quantity; the effect of measuring it dynamically at finite frequency  $\omega$  is to introduce a length scale over which the system is probed. In models with vortex proliferation this is typically proportional to the vortex diffusion length  $\sqrt{D/\omega}$ , where  $D$  is a vortex diffusion constant.

<sup>1</sup>The Institute for Quantum Matter, Department of Physics and Astronomy, The Johns Hopkins University, Baltimore, Maryland 21218, USA, <sup>2</sup>Brookhaven National Laboratory, Upton, New York 11973, USA. \*e-mail: npa@pha.jhu.edu.

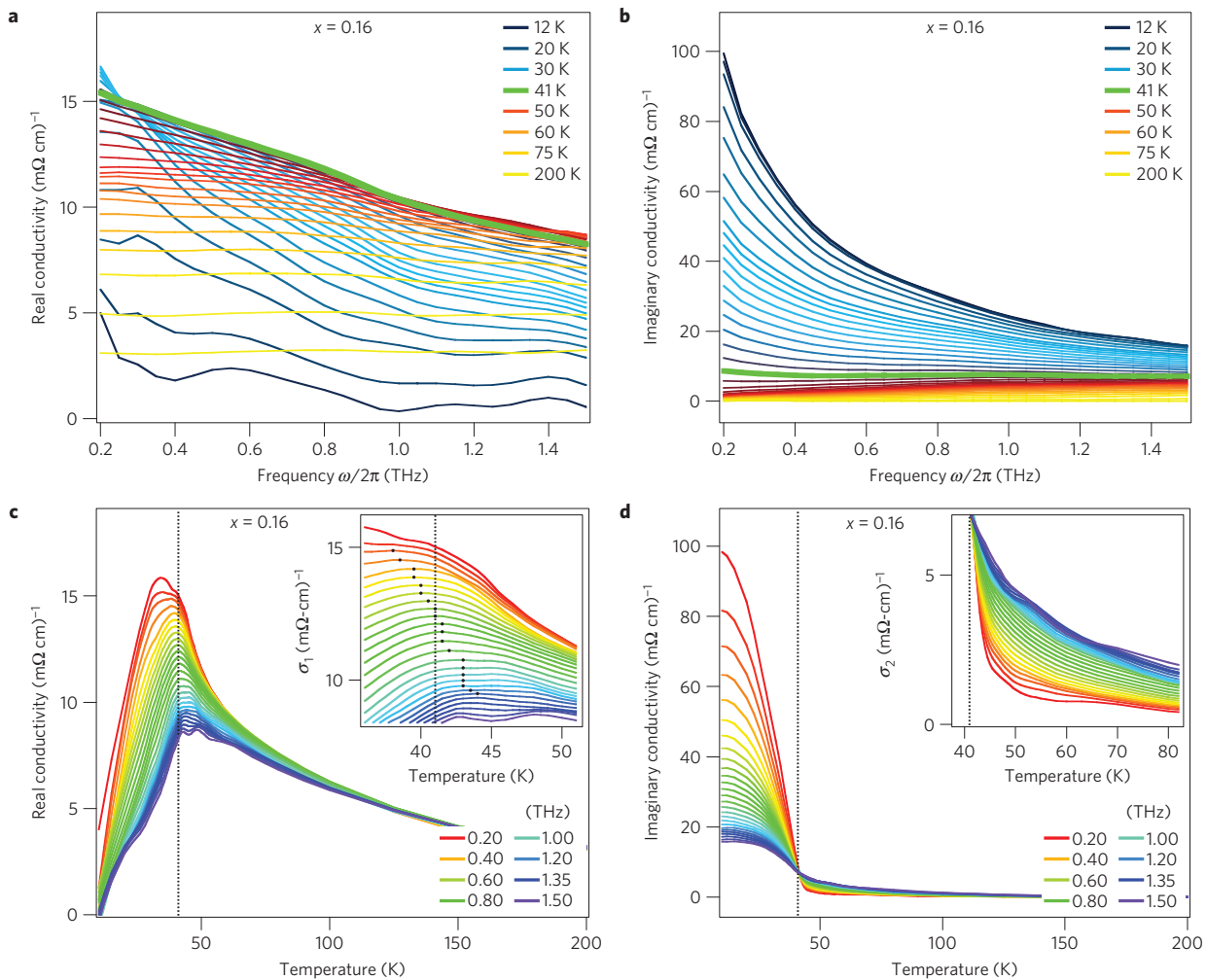


**Figure 1 | THz conductivity of an  $x = 0.16$   $\text{La}_{2-x}\text{Sr}_x\text{CuO}_4$  thin film.** **a,b**, Real and imaginary conductivities as a function of frequency at different temperatures for an optimally doped  $x = 0.16$  sample ( $T_c = 41$  K). **c,d**, Real and imaginary conductivities as a function of temperature at different frequencies for  $x = 0.16$ . In **a** and **b** the green curve denotes  $T_c$ . In **c** and **d** the vertical lines represent  $T_c$ . Insets to **c** and **d** show expanded views of the fluctuation region. Black dots mark the approximate peak value in the inset to **c**.

In Fig. 2, we plot the quantity  $\omega\sigma_2$  as a function of frequency and temperature in a and b, respectively, for an underdoped sample ( $x = 0.09$ ) with  $T_c = 22$  K. This quantity is proportional to the phase stiffness  $T_\phi$  when the superconducting signal dominates over the normal-state background. Owing to uncertainties in its possible form, we have abstained from subtracting a background from the plotted signal. We find, however, that different choices for backgrounds have little effect on our conclusions. Deep in the superconducting state, there is essentially no frequency dependence to  $\omega\sigma_2$ , which is consistent with the fact that the system's phase is 'stiff' on all length scales. At higher temperatures the curves in Fig. 2b spread as a frequency dependence is acquired. Interestingly, the temperature where the spreading first becomes significant is very close to the temperature where the Kosterlitz–Thouless–Berezinskii (KTB) theory (black dashed line) would predict a discontinuous jump in this quantity for an isolated  $\text{CuO}_2$  plane<sup>18</sup>. LSCO is of course only a quasi-two-dimensional system, but the fact that we observe a spreading at the KTB prediction shows that at some temperature  $T_{\text{KTB}}^{\text{eff}} < T_c$  there begin to be significant fluctuations of a two-dimensional character even below the transition.  $T_c$  itself does not occur until higher temperatures, as it is controlled by three-dimensional couplings. All of our underdoped samples, as well as previous measurements of BSCCO films<sup>11</sup>, show this behaviour. As shown by the frequency

dependence of  $\omega\sigma_2$  above  $T_{\text{KTB}}^{\text{eff}}$ , the fluctuations first degrade the stiffness on long length and timescales, that is, low frequencies. To compare across the phase diagram, in Fig. 2c we plot  $\omega\sigma_2$  for many dopings at a frequency 0.8 THz. Qualitatively, we regard the onset temperature  $T_o$  as the temperature where the quantity  $\omega\sigma_2$  presents a substantial deviation from the trend of the higher-temperature normal state. As a quantitative measure, we find that all samples exhibit a very sharp deviation out of the smooth high-temperature signal in this range in plots of the second derivative (Fig. 2d) versus temperature. We take this deviation as the quantitative measure of  $T_o$  (with error bars). For all dopings,  $T_o$  is no more than 16 K above  $T_c$ . It is also interesting to note that the difference between  $T_o$  and  $T_c$  is relatively constant over the experimental range.

As mentioned above, the data in Figs 1 and 2 are consistent with superconducting correlations that are typified by a slowing down of the characteristic fluctuation rates as temperature is decreased. In general, the diverging length and timescales near a continuous phase transition lend themselves to a scaling analysis in which response functions can be written in terms of these diverging scales. Close to a superconducting transition we expect that the relation

$$\sigma_f(\omega) = \frac{G_Q}{t} \frac{k_B T_\phi^0}{\hbar\Omega} S\left(\frac{\omega}{\Omega}\right) \quad (1)$$

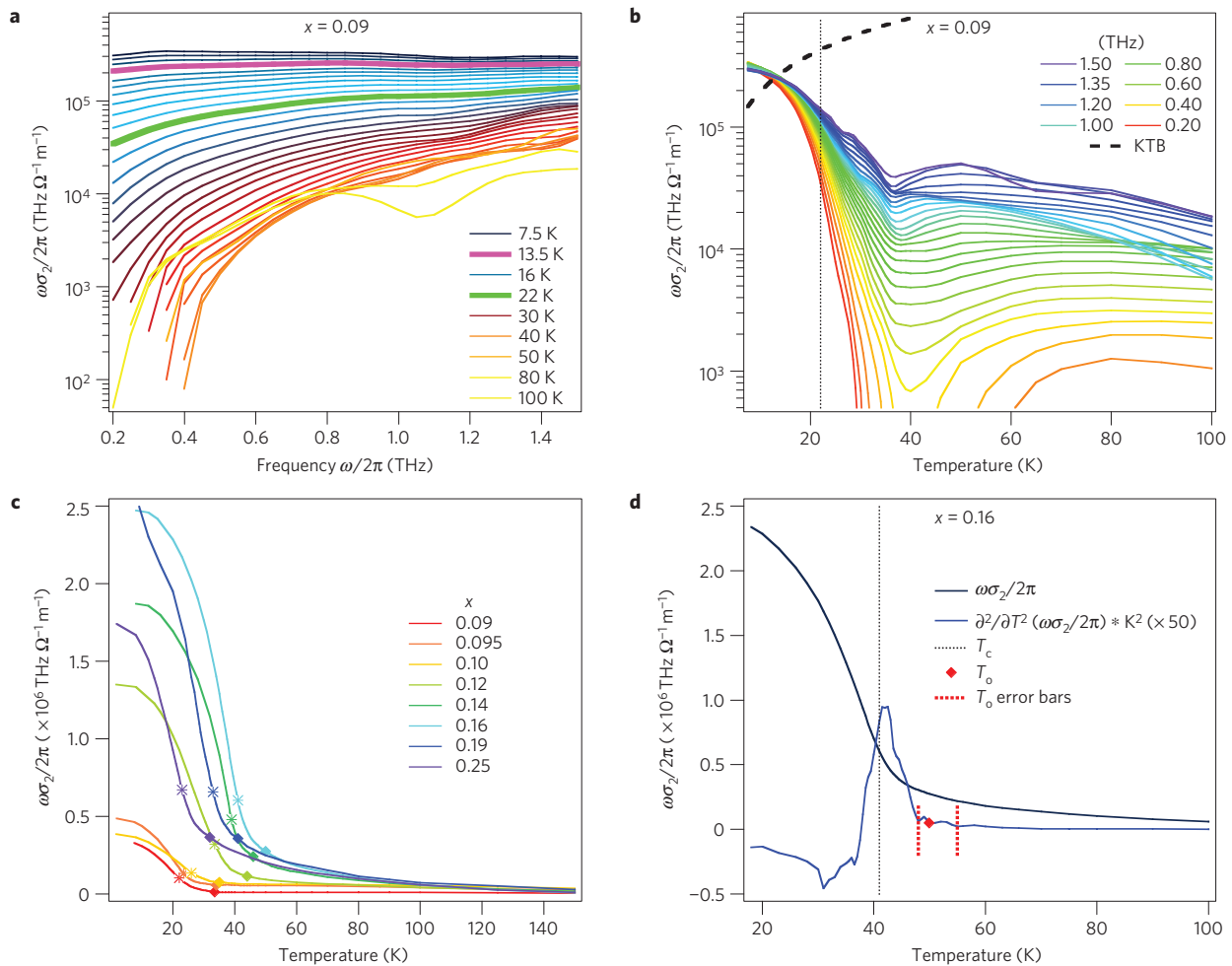


**Figure 2** |  $\omega\sigma_2$  is proportional to the THz ‘phase stiffness’. **a**,  $\omega\sigma_2$  versus frequency at different temperatures for the  $x = 0.09$  underdoped sample ( $T_c = 22$  K). The green curve denotes  $T_c$ . The pink curve is the effective KTB temperature. **b**,  $\omega\sigma_2$  as a function of temperature for different frequencies for the  $x = 0.09$  underdoped sample. The bold dashed black line is the prediction of the KTB transition for a single isolated  $\text{CuO}_2$  plane. The temperature of its crossing with the experimental data defines an effective KTB temperature. The vertical line represents  $T_c$ . **c**,  $\omega\sigma_2$  at 800 GHz at a number of different dopings.  $T_c$  is indicated by the asterisks and  $T_0$  is indicated by diamonds. **d**,  $T_0$  (red diamond) and error bars (red lines), as defined for the  $x = 0.16$  sample by the onset of curvature of  $\omega\sigma_2$ .

holds for the portion of the conductivity due to superconducting fluctuations  $\sigma_f$ . Here  $T_\phi^0$  is a temperature-dependent prefactor and  $\Omega$  is the characteristic fluctuation rate. Temperature dependencies enter only through the quantities  $\Omega$  and  $T_\phi^0$ . This scaling function is similar to the one proposed by Fisher, Fisher and Huse<sup>19</sup> and is identical to the one used in previous THz measurements on underdoped BSCCO (ref. 11). Note that equation (1) is a very general form that does not assume any particular dimensionality of the system or character (vortex, Gaussian and so on) of the fluctuations or functional dependencies on temperature of  $\Omega$  and  $T_\phi^0$ . Also note that although the fluctuation conductivity  $\sigma_f = |\sigma_f|e^{i\varphi}$  is a complex quantity all prefactors to the  $S$  scaling function are real and therefore the phase of  $S$  is equal to the phase of  $\sigma_f$ .  $S$  is expected to exhibit single-parameter scaling and thus a collapse of  $\varphi$  measured at different temperatures as a function of the reduced frequency  $\omega/\Omega$  yields the temperature-dependent  $\Omega$ . In Fig. 3a, we show the collapsed phase  $\varphi = \tan^{-1}\sigma_2/\sigma_1$  of the  $x = 0.16$  sample as a function of the reduced frequency  $\omega/\Omega$  for 45 different temperatures in the 30–55 K range. As expected, the phase is an increasing function of  $\omega/\Omega$ , with the metallic limit  $\varphi = 0$  reached at  $\omega/\Omega \rightarrow 0$  and  $\varphi$  becoming large (but bounded by  $\pi/2$ ) as  $\omega/\Omega \rightarrow \infty$ .

We were able to carry out the scaling analysis and obtain similarly good data collapse for all eight samples in the range  $x = 0.09$ – $0.25$ . In Fig. 3b we plot their extracted fluctuation rates  $\Omega$  as a function of temperature. In almost all samples the fluctuation rate increases very quickly (almost exponentially) within 10 K of  $T_c$ . Note that the characteristic fluctuation frequency  $\Omega$  is actually smooth through  $T_c$ , in a manner quite different than expected from the Fisher–Fisher–Huse scaling, and it seems to extrapolate to zero near the effective  $T_{\text{KTB}}^{\text{eff}}$ , where two-dimensional-like fluctuations become strong. At a temperature we denote as  $T_Q$ , the extracted fluctuation rate crosses over to a regime where it grows at a much smaller rate, which is proportional to temperature as  $\alpha k_B T/\hbar$ . As the resistivity itself is linear in  $T$  (see Supplementary Information),  $T_Q$  is an alternative measure of the temperature scale where we cannot distinguish superconducting fluctuations from normal-state transport. Interestingly, we continue to obtain good scaling and data collapse as we continue the analysis for another 5–10 K above  $T_Q$ . This behaviour may be related to the  $\omega/T$  scaling that has been seen in the normal state<sup>20</sup>.

In Fig. 4 we construct a phase diagram of the fluctuation regime summarizing our results. We compare  $T_c$  of films and bulk crystals, the diamagnetism onset from ref. 10, the region of THz conductivity onset  $T_0$  (as defined by the sudden change in curvature of  $\omega\sigma_2$

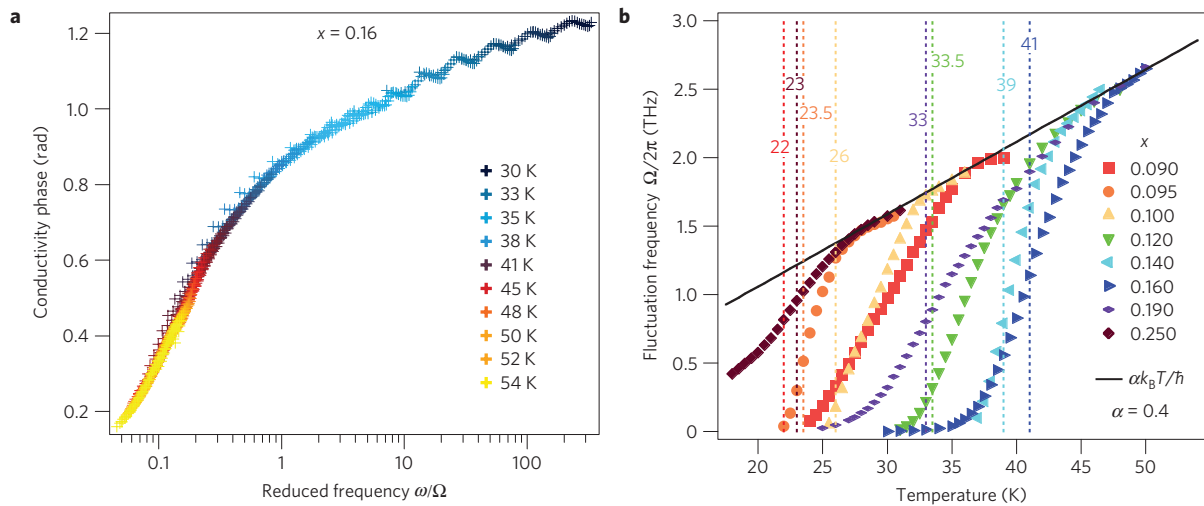


**Figure 3 | Characteristic fluctuation frequency obtained through a scaling analysis.** **a**, Phase of the conductivity  $\varphi = \tan^{-1} \sigma_2 / \sigma_1$  in the frequency range from 0.5 THz to 1.5 THz as a function of the reduced frequency for 45 different temperatures in the range of 30–55 K for the  $x = 0.16$  sample. **b**, The superconducting fluctuation rate  $\Omega(T)$  determined as detailed in the text for a variety of different dopings. Coloured vertical lines are the  $T_c$  values for the respective dopings. It is observed that the fluctuation rate for all dopings approaches a limiting linear temperature dependence.

from Fig. 2d) and  $T_Q$ , where  $\Omega$  begins to grow linearly with temperature. Unsurprisingly, to within experimental uncertainty  $T_Q$  and  $T_o$  track each other. For all dopings the THz fluctuation conductivity shows an onset between 5 K and 16 K above  $T_c$ . This is in strong contrast to measurements such as diamagnetism, where the signal persists in similar samples to almost 100 K above  $T_c$ . Although fluctuation diamagnetism is a thermodynamic quantity sensitive to spatial correlations and THz conductivity a dynamical quantity sensitive to temporal correlations, the differences are still surprising, as within most models based on diffusive dynamics we expect a close correspondence between them<sup>18</sup>. An approximately 20 K difference in the onset temperatures exists between diamagnetism and previous THz measurements on BSCCO (refs 11,21), but the present 80 K discrepancy is much larger (particularly when normalized to the respective  $T_c$  values) and cannot be easily explained away.

We may draw a few possible conclusions. One obvious possibility is that there is little correspondence of diamagnetism (and Nernst effect) to conductivity because the former class of measurements is sensitive to something other than only superconductivity well above  $T_c$ . In this regard, it has been shown recently that the onset of density-wave order can give a strong Nernst response<sup>9</sup>, and that bond current states can in principle exhibit enhanced diamagnetism<sup>22</sup>. However, if the diamagnetism signal above  $T_o$  is solely due to superconducting correlations then it is a well-posed theoretical challenge to explain the lack of straightforward correspondence to conductivity.

We have found that at some temperature  $T_Q > T_c$  the fluctuation rate  $\Omega$  is either overwhelmed by the linear-in- $T$  normal-state scattering rate or becomes linear in  $T$  itself. Calculations that model the normal state as a vortex liquid<sup>23–25</sup> with a characteristic dissipation rate proportional to  $T$  favour the latter scenario. Unfortunately, our measurements cannot distinguish these possibilities. It is interesting to note that the regime in which we observe a large fluctuation conductivity is essentially the same as the regime of ‘fragile London rigidity’ in the diamagnetism of Li *et al.*<sup>10,21</sup>. It may be that there are two distinct types of superconducting fluctuation, one of which gives a divergent or near-divergent contribution to the susceptibility in a relatively narrow range of temperatures above  $T_c$  and the other of which gives a more extended, but less spectacular, contribution to the susceptibility. If the first type

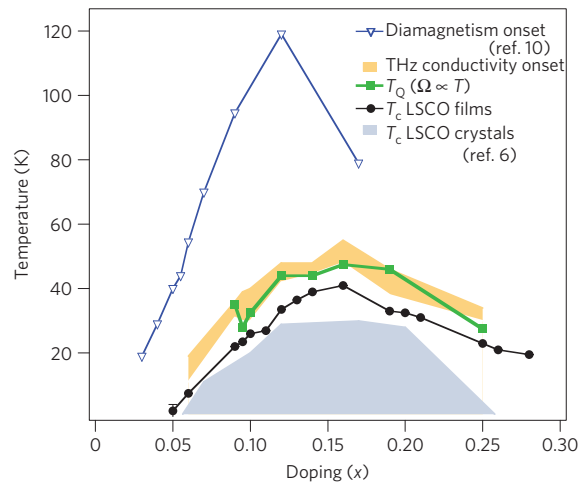


**Figure 4 | Phase diagram of the onset of superconducting correlations in LSCO.** Temperature-versus-doping phase diagram of  $\text{La}_{2-x}\text{Sr}_x\text{CuO}_4$  comparing  $T_c$  of thin films and bulk crystals with the THz conductivity onset  $T_o$  and the diamagnetism onset temperature from ref. 10. Here,  $T_o$  is expressed as a shaded region to convey the uncertainty in its determination. The temperature  $T_Q$  at which the characteristic fluctuation rate  $\Omega$  becomes proportional to temperature is plotted in green.

makes a more significant contribution to the conductivity than the second, this may resolve the apparent conflict between the two probes. Similarly, the differences may arise in how the quantities in question depend on correlations in space (probed by diamagnetism) versus correlations in time (probed by conductivity). As noted above, within classical diffusive dynamics, we generally expect a correspondence between these quantities. Our data show that if the regime of enhanced diamagnetism is due to superconductivity then a very unconventional relationship must exist between length and time correlations in the fluctuation superconductivity. Among other possibilities, this could arise from phase separation<sup>26</sup>, unusually fast vortices<sup>27,28</sup> or the presence of explicitly quantum diffusion. Whatever the reason, our data show that superconducting fluctuations do not make an appreciable contribution to the charge-transport anomalies in the pseudogap regime at temperatures well above  $T_c$ .



## Methods

The complex conductivity was determined by time-domain THz spectroscopy. A femtosecond laser pulse is split along two paths and excites a pair of photoconductive 'Auston'-switch antennae grown on radiation-damaged silicon on sapphire wafers. A broadband THz-range pulse is emitted by one antenna, transmitted through the LSCO film and measured at the other antenna. By varying the length difference of the two paths, we map out the entire electric field of the transmitted pulse as a function of time. Comparing the Fourier transform of the transmission through LSCO with that of a reference resolves the full complex transmission. We then invert the transmission to obtain the complex conductivity through the standard formula for thin films on a substrate:  $\hat{T}(\omega) = (1+n)/(1+n+Z_0\sigma(\omega)d)e^{i\Phi_s}$ , where  $\Phi_s$  is the phase accumulated from the small difference in thickness between the sample and reference substrates,  $n$  is the substrate index of refraction,  $Z_0 = 377 \Omega$  is the impedance of free space and  $d$  is the thin-film thickness. By measuring both the magnitude and phase of the transmission, this inversion to conductivity is done directly and does not require Kramers–Kronig transformation.

Our scaling analysis includes some uncertainty in setting the overall scale of  $\Omega$ , as equation (1) only specifies  $\Omega$  up to a numerical factor. We set the overall scale of  $\Omega$  so that the loss peak in Fig. 1c is exhibited at a temperature where the probing frequency  $\omega$  is equal to the fluctuation frequency  $\Omega$  at that temperature. This is an imprecise procedure and applying it strictly gives a small distribution (40%) in the values of  $\alpha$  for different dopings. We choose the normalizations for the data plotted in Fig. 3 such that  $\alpha = 0.4$ , which is the mean value for all the data. We take the relatively small spread in  $\alpha$  values as evidence of the veracity of our procedure, but emphasize that the  $\alpha$  values could be revised with a different criterion for the scale factors. As a cross-check we also fit the conductivity using a Kramers–Kronig consistent fitting routine<sup>29</sup> and obtain good agreement above  $T_c$  between the half-width of the Lorentzian peak used to model the fluctuation contribution and the rates given in Fig. 3b.

The LSCO films were deposited on 1-mm-thick single-crystal LaSrAlO<sub>4</sub> substrates, epitaxially polished perpendicular to the (001) direction, by atomic layer-by-layer molecular beam epitaxy<sup>30</sup>. The samples were characterized by reflection high-energy electron diffraction, atomic force microscopy, X-ray diffraction, and resistivity and magnetization measurements, all of which indicate excellent film quality. For accurate determination of the conductivity, it is critical to know the film thickness accurately. This was measured digitally by counting atomic layers and reflection high-energy electron diffraction oscillations, as well as from so-called Kiessig fringes in small-angle X-ray reflectance and from finite thickness oscillations observed in X-ray diffraction patterns. The  $x = 0.14$ , 0.16 and 0.25 films are 80 monolayers thick; the  $x = 0.095$  and 0.19 films are 114 monolayers; the  $x = 0.09$ , 0.10 and 0.12 films are 150 monolayers (one monolayer is  $\approx 6.6 \text{ \AA}$ ).

Received 11 August 2010; accepted 21 December 2010;  
published online 13 February 2011

## References

1. Timusk, T. & Statt, B. The pseudogap in high-temperature superconductors: An experimental survey. *Rep. Prog. Phys.* **62**, 61–122 (1999).
2. Damaschelli, A., Hussain, Z. & Shen, Z. X. Angle-resolved photoemission studies of the cuprate superconductors. *Rev. Mod. Phys.* **75**, 473–541 (2003).
3. Norman, M., Pines, D. & Kallin, C. The pseudogap: Friend or foe of high  $T_c$ ? *Adv. Phys.* **54**, 715–733 (2005).
4. Uemura, Y. J. *et al.* Basic similarities among cuprate, bismuthate, organic, Chevrel-phase, and heavy-fermion superconductors shown by penetration-depth measurements. *Phys. Rev. Lett.* **66**, 2665–2668 (1991).
5. Emery, V. & Kivelson, S. Importance of phase fluctuations in superconductors with small superfluid density. *Nature* **374**, 434–437 (1995).
6. Wang, Y., Li, L. & Ong, N. P. Nernst effect in high- $T_c$  superconductors. *Phys. Rev. B* **73**, 024510 (2006).
7. Wang, Y. *et al.* Field-enhanced diamagnetism in the pseudogap state of the cuprate Bi<sub>2</sub>Sr<sub>2</sub>CaCu<sub>2</sub>O<sub>8+ $\delta$</sub>  superconductor in an intense magnetic field. *Phys. Rev. Lett.* **95**, 247002 (2005).
8. Lee, P. A., Nagaosa, N. & Wen, X. G. Doping a Mott insulator: Physics of high-temperature superconductivity. *Rev. Mod. Phys.* **78**, 17–85 (2006).
9. Cyr-Choinière, O. *et al.* Enhancement of the Nernst effect by stripe order in a high- $T_c$  superconductor. *Nature* **458**, 743–745 (2009).
10. Li, L. *et al.* Diamagnetism and Cooper pairing above  $T_c$  in cuprates. *Phys. Rev. B* **81**, 054510 (2010).
11. Corson, J., Mallozzi, R., Orenstein, J., Eckstein, J. N. & Bozovic, I. Vanishing of phase coherence in underdoped Bi<sub>2</sub>Sr<sub>2</sub>CaCu<sub>2</sub>O<sub>8+ $\delta$</sub> . *Nature* **398**, 221–223 (1999).

12. Crane, R. *et al.* Survival of superconducting correlations across the two-dimensional superconductor-insulator transition: A finite-frequency study. *Phys. Rev. B* **75**, 184530 (2007).
13. Xu, Z. A., Ong, N. P., Wang, Y., Kakeshita, T. & Uchida, S. Vortex-like excitations and the onset of superconducting phase fluctuation in underdoped La<sub>2-x</sub>Sr<sub>x</sub>CuO<sub>4</sub>. *Nature* **406**, 486–488 (2000).
14. Kitano, H., Ohashi, T., Maeda, A. & Tsukada, I. Critical microwave-conductivity fluctuations across the phase diagram of superconducting La<sub>2-x</sub>Sr<sub>x</sub>CuO<sub>4</sub> thin films. *Phys. Rev. B* **73**, 092504 (2006).
15. Grbić, M. S. *et al.* Microwave measurements of the in-plane and  $c$ -axis conductivity in HgBa<sub>2</sub>CuO<sub>4+ $\delta$</sub> : Discriminating between superconducting fluctuations and pseudogap effects. *Phys. Rev. B* **80**, 094511 (2009).
16. Grbić, M. S. *et al.* Temperature range of superconducting fluctuations above  $T_c$  in YBa<sub>2</sub>Cu<sub>3</sub>O<sub>7- $\delta$</sub>  single crystals. Preprint at <http://arxiv.org/abs/1005.4789v2> (2010).
17. Maeda, A., Nakamura, D., Shibuya, Y., Imai, Y. & Tsukada, I. THz conductivity of La<sub>2-x</sub>Sr<sub>x</sub>CuO<sub>4</sub> in the pseudogap region and in the superconductivity state. *Physica C* **470**, 1018–1020 (2010).
18. Halperin, B. I. & Nelson, D. R. Resistive transition in superconducting films. *J. Low Temp. Phys.* **36**, 599–616 (1979).
19. Fisher, D. S., Fisher, M. P. A. & Huse, D. A. Thermal fluctuations, quenched disorder, phase transitions, and transport in type-II superconductors. *Phys. Rev. B* **43**, 130–159 (1991).
20. Molegraaf, H. J. A., Presura, C., van der Marel, D., Kes, P. H. & Li, M. Superconductivity-induced transfer of in-plane spectral weight in Bi<sub>2</sub>Sr<sub>2</sub>CaCu<sub>2</sub>O<sub>8+ $\delta$</sub> . *Science* **295**, 2239–2241 (2002).
21. Li, L. *et al.* Strongly nonlinear magnetization above  $T_c$  in Bi<sub>2</sub>Sr<sub>2</sub>CaCu<sub>2</sub>O<sub>8+ $\delta$</sub> . *Europhys. Lett.* **72**, 451–457 (2005).
22. Sau, J. D. & Tewari, S. Diamagnetism from the 6-vertex model and implications for the cuprate superconductors. Preprint at <http://arxiv.org/abs/1009.5926v2> (2010).
23. Vafek, O. & Tešanović, Z. Quantum criticality of  $d$ -wave quasiparticles and superconducting phase fluctuations. *Phys. Rev. Lett.* **91**, 237001 (2003).
24. Melikyan, A. & Tešanović, Z. Model of phase fluctuations in a lattice  $d$ -wave superconductor: Application to the Cooper-pair charge-density wave in underdoped cuprates. *Phys. Rev. B* **71**, 214511 (2005).
25. Anderson, P. W. Bose fluids above  $T_c$ : Incompressible vortex fluids and 'supersolidity'. *Phys. Rev. Lett.* **100**, 215301 (2008).
26. Martin, I. & Panagopoulos, C. Nernst effect and diamagnetic response in a stripe model of superconducting cuprates. *Europhys. Lett.* **91**, 67001 (2010).
27. Ioffe, L. B. & Millis, A. J. Big fast vortices in the  $d$ -wave resonating valence bond theory of high-temperature superconductivity. *Phys. Rev. B* **66**, 094513 (2002).
28. Lee, P. A. Orbital currents and cheap vortices in underdoped cuprates. *Physica C* **388–389**, 7–10 (2003).
29. Kuzmenko, A. B. Kramers–Kronig constrained variational analysis of optical spectra. *Rev. Sci. Instrum.* **76**, 083108 (2005).
30. Bozovic, I. Atomic-layer engineering of superconducting oxides: Yesterday, today, tomorrow. *IEEE Trans. Appl. Supercon.* **11**, 2686–2695 (2001).

## Acknowledgements

The authors would like to thank P. W. Anderson, A. Auerbach, A. Dorsey, N. Drichko, S. Kivelson, L. Li, W. Liu, V. Oganesyan, N. P. Ong, J. Orenstein, F. Ronning, O. Tchernyshyov, Z. Tešanović, A. Tselvik, D. van der Marel and J. Zaanen for discussions and/or correspondence. Support for the measurements at The Johns Hopkins University was provided under the auspices of the Institute for Quantum Matter, Department of Energy DE-FG02-08ER46544. The work at Brookhaven National Laboratory was supported by the US Department of Energy under project No MA-509-MACA.

## Author contributions

L.S.B. designed and built the THz spectrometer; L.S.B. and R.V.A. made the THz measurements; L.S.B. analysed the data; G.L. and I.B. synthesized the films (using reflection high-energy electron diffraction for *in situ* characterization) and measured mutual inductance; O.P. took the X-ray diffraction and atomic force microscopy data; L.S.B., R.V.A., I.B. and N.P.A. wrote and revised the manuscript; N.P.A. devised the experiment.

## Additional information

The authors declare no competing financial interests. Supplementary information accompanies this paper on [www.nature.com/naturephysics](http://www.nature.com/naturephysics). Reprints and permissions information is available online at <http://npg.nature.com/reprintsandpermissions>. Correspondence and requests for materials should be addressed to N.P.A.